JOINT INSTITUTE FOR NUCLEAR RESEARCH

Veksler and Baldin Laboratory of High Energy Physics

FINAL REPORT ON THE START PROGRAMME

FLUKA/FLAIR Simulation-Based Assessment of Absorbed Dose from ^{131}Xe Heavy-Ion Irradiation Using Solid-State Samples for Material Science Applications

Supervisor:
Dr. Nelli Pukhaeva

Student:
Tendani Oliver Munyai

Dubna, Russia, 2025

Acknowledgement

I have always wanted to study at JINR in order to extend my knowledge. It certainly has not disappointed. I would firstly like to extend my heartfelt gratitude to the Almighty God for granting me the strength, wisdom, and perseverance throughout the completion of this study.

I am deeply indebted to my supervisor, **Dr. Nelli Pukhaeva**, for her invaluable guidance, encouragement, and support throughout this work. I owe my sincere thanks to my supervisor **Prof Suzan Bvumbi** for checking up on me throughout this study.

My sincere appreciation also goes to my colleague **Adam Lahera**, who was always present and supportive during this journey, and to **Kanat**, whose guidance and advice were instrumental in shaping my understanding and progress. I would also love to thank sophia for her good hospitality.

Finally, I would like to express my profound gratitude to the **Joint Institute for Nuclear Research (JINR)** and **NICA** for selecting me to be part of the world-renowned **START programme**, one of the biggest and most impactful scientific programs globally. This opportunity has been a remarkable milestone in my academic and research path.

Abstract

This study used Monte Carlo simulations with the FLUKA/FLAIR code to analyze how heavy xenon ions deposit energy in solid samples. The main goal was to calculate the absorbed dose and understand the efficiency of the beam setup. A beam of ^{131}Xe ions at 3.8 GeV was simulated as it passed through detectors and a composite sample made of Ag/$YBa_2Cu_3O_7$/MgO/Hastelloy. The results showed that only 31.53% of the beam reached the sample. The absorbed dose was calculated as 4.44×10^{-8} Gy. These results highlight inefficiencies in the current setup and suggest improvements such as vacuum beamlines, large samples, and collimators for better focusing. The study shows how FLUKA/FLAIR can be used effectively for absorbed dose studies in materials, with relevance to nuclear physics, radiation protection, and medical applications.

Keywords: Monte Carlo simulation, FLUKA, FLAIR, absorbed dose,

Contents

List of Tables

List of Figures

1 Literature Review

1.1 Introduction

This work focused on analysing the beam intensity of absorbed dose in solid materials. However, heavy ions are charged nuclei whose mass is greater than that of helium-4 (^{4}He) [1]. One example of a heavy ion is $^{124}Xe^{54+}$. Heavy ions are considered efficient because they transfer a large amount of energy to solid materials [2, 3]. In addition, they exhibit a high relative biological effectiveness (RBE) [1]. Their use in particle, nuclear, and biological physics continues to be significant. Therefore, the use of high ion beams for irradiating solid materials was the main emphasis of this work.

1.2 Review on ARIADNA and NICA Projects in the Context of Irradiated Radiobiological Samples by Heavy Ions

The ARIADNA (Applied Research Infrastructure for Advanced Developments at NICA Facility) project is part of the larger NICA (Nuclotron-based Ion Collider Facility) in Dubna, Russia, which is a large-scale research facility that operates as a powerful source for accelerating and colliding beams of various ions (charged atoms). The ARIADNA project focused on applying these ion beams for practical experiments, not solely theoretical investigations. A major emphasis was placed on studying the effects of heavy ion beams on biological systems.

A dedicated irradiation station was used for exposing biological samples such as cells, proteins, and DNA to these ion beams. Different types of ions, ranging from light ones like carbon to heavy ones like gold, could be accelerated to different energy levels. This versatility was particularly useful because it allowed simulations of space radiation conditions, which is important for ensuring astronaut safety during long-term missions.

To investigate the effects, advanced experimental techniques were employed. For instance, specially engineered cells that emitted fluorescence upon radiation damage were used. This glow served as an alarm system, indicating the extent of radiation-induced damage. Moreover, studies of localized damage caused by a single ion striking a protein crystal provided insight into the fundamental processes of radiation damage at the microscopic scale.

Such research not only contributed to developing protective strategies for astronauts exposed to cosmic radiation but also enhanced the effectiveness of cancer treatment through ion therapy, making it more precise and efficient [4, 5].

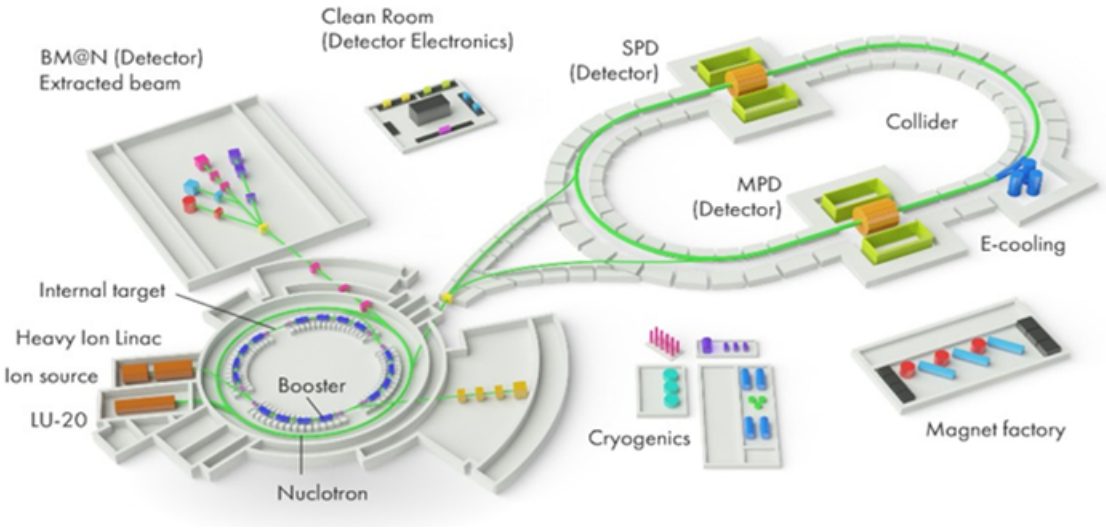

Figure 1: Scheme of the structure of the NICA Complex [21]

1.3 Beamline and Detector Systems

The process began at the ion source, where heavy ions were produced. These ions were then injected into and accelerated by the Heavy Ion Linear Accelerator (LU-20). From there, the beam could be directed to the Booster ring, where ions were accumulated and their energy was further increased. The accelerated beam was subsequently transferred to the main accelerator, the Nuclotron, a superconducting synchrotron that accelerated ions to their final high energies [6].

Once accelerated, the beams were delivered to the Multi-Purpose Detector (MPD) and the Spin Physics Detector (SPD) to study head-on collisions of two counter-rotating beams of ions. Alternatively, an extracted beam could be directed to the BM@N (Baryonic Matter at Nuclotron) experiment, which studied collisions with a stationary internal target [7,8]. The present study focused on collisions involving a stationary internal sample.

1.3.1 BM@N Experiment

The BM@N experiment was a fixed-target experiment conducted at the NICA-Nuclotron accelerator complex at the Joint Institute for Nuclear Research (JINR) in Dubna, Russia. Its primary objective was to study interactions of relativistic heavy-ion beams with energies up to 5 AGeV per nucleon using fixed targets. The focus was on the production of strange mesons, multi-strange hyperons, and light hypernuclei near kinematic thresholds.

The experimental setup featured a sophisticated spectrometer centered around a dipole magnet and included a high-precision central tracker based on triple GEM (Gas Electron Multiplier) detectors, drift and cathode pad chambers, time-of-flight detectors using multi-gap resistive plate chambers (mRPC), and calorimeters for collision centrality and electromagnetic probes. A technical run conducted in 2016 with a deuteron beam successfully commissioned the detector systems and enabled the reconstruction of Λ-hyperons

via their decay into proton–pion pairs, validating both the detection methodology and Monte Carlo simulations [7,8].

1.4 Relevance of 3.8 GeV/nucleon $^{124}Xe^{54+}$ Beams for Absorbed Dose Studies

The study by P. I. Zarubin et al. [9] provided evidence of the use of 3.8 GeV/nucleon $^{124}Xe^{54+}$ beams at the NICA facility, demonstrating their suitability for absorbed dose studies in solid materials. Their primary objective was to quantify the beam intensity and to visualize the beam profile, while another objective was to investigate beam propagation characteristics.

Nuclear Photo-Emulsion (NTE) samples were irradiated by $^{124}Xe^{54+}$ ions. The samples were analyzed using microscopes to scan the entire surface, acquire thousands of images, and count every individual track. This enabled the creation of a detailed map showing where the beam struck and its intensity at each point. Distinct tracks of xenon ions tearing through the emulsion film were observed, accompanied by delta-electron production. Notably, instances of xenon nuclei directly colliding with target nuclei were recorded.

The results showed that 3.8 GeV/nucleon $^{124}Xe^{54+}$ ions penetrated deeply into the materials, producing continuous tracks across the full thickness of the samples. At points of collision, scattering led to secondary nuclear fragments, visible as multiple smaller tracks branching from the original trajectory. These findings demonstrated that such beams deposit high-density ionization and induce nuclear fragmentation, making them highly suitable for absorbed dose investigations in solid samples. Consequently, the present study employed 3.8 GeV/nucleon $^{124}Xe^{54+}$ beams for irradiation of solid materials.

1.5 Ionization Chamber

An ionization chamber is a detector used to measure the intensity of ionizing radiation, such as ion beams, by collecting the electrical charge generated when radiation interacts with a gas inside the chamber [10]. It has been widely adopted in nuclear physics, medical physics, and radiation protection due to its stability and ability to provide precise measurements across a wide range of radiation levels.

McEwen et al. [11] conducted a detailed study to examine the influence of humidity on the performance of a reference ionization chamber. The chamber was placed inside a controlled environment where humidity could be adjusted from extremely dry to very humid conditions. Their results demonstrated that humidity had no significant effect on the detector's response. Regardless of atmospheric moisture levels, the chamber consistently delivered accurate readings [11].

This robustness highlights the reliability of ionization chambers, as they can function effectively under varying environmental conditions without loss of accuracy. Such stability is particularly important for experiments requiring long-term monitoring and consistency of data. For these reasons, the present study employed ionization chambers as the primary detectors for beam intensity measurements.

Figure 2: Ionization chamber

1.6 Concept of Absorbed Dose

Absorbed dose is the energy deposited by ionizing radiation per unit mass of a material [12]. It is expressed in Gray (Gy), where 1 Gy = 1 Joule per kilogram ($1\,\mathrm{Gy} = 1\,\mathrm{J/kg}$) [13]. The measurement of absorbed dose is significant in many domains, including medical radiation therapy, radiation protection, and nuclear research, because it reflects both the biological and physical impacts of radiation exposure [14].

The absorbed dose D at a certain site in any given volume is defined as follows [13, 14]:

$$D = \frac{d\varepsilon}{dm}$$

where:

- $d\varepsilon$ is the mean energy imparted to matter in a volume element dv,
- dm is the mass of that volume element.

1.7 Characterization of Ion Beams

It was very important that an ion beam spread out evenly across the target. Otherwise, some spots would have received more radiation than others, reducing the efficiency of the experiment. To check this, detectors were used to measure the beam's spatial distribution. For example, Filatov et al. [15] used a special film that changed colour where the beam

struck it. After the experiment, the colour distribution on the film was analyzed to determine beam uniformity.

Another key parameter was the number of ions striking the target per unit time. Faraday cups and ionization chambers were used for this purpose. These detectors caught the incoming ions and measured their charge, thereby estimating the beam's intensity [15]. Filatov et al. [15] also showed that high-energy ions penetrated deeply into materials, whereas low-energy ions stopped closer to the surface. The beam energy determined the interaction mechanism: high-energy ions could knock atoms out of place (nuclear stopping), while lower energy transfer excited and broke atomic bonds (electronic stopping) [15, 16].

1.7.1 Concept of Ion Fluence and Exposure Duration

Fluence is the total number of ions incident on a unit area of a target, expressed in ions/cm^2 [16]. It represents the radiation dose delivered to the material [12, 16]. Wang et al. [17] discussed exposure duration as the total time over which an ion beam irradiated a target. As reported by Filatov et al. [15] and Chen et al. [16], a higher fluence could be achieved only by increasing the exposure duration, showing that ion fluence was directly proportional to irradiation time. In this study, the relationship between exposure duration and fluence was analyzed to determine the absorbed dose on the sample.

1.8 Monte Carlo Simulations for Dose

P. N. Ostroumov et al. [18] analyzed the widely used SRIM code but highlighted its limitations. SRIM was slow and impractical for simulations tracking millions of particles. It was also restricted to low- and medium-energy regimes (eV to MeV), making it unsuitable for high-energy (GeV) beams. For this reason, FLUKA was preferred due to its ability to handle GeV-scale simulations accurately and efficiently.

1.8.1 FLUKA and FLAIR in Absorbed Dose Simulation

The FLUKA Monte Carlo code is a multipurpose computational tool developed by CERN and INFN for simulating radiation transport and interactions. It supports hadrons, heavy ions, and electromagnetic particles, using highly refined physics models [16]. Its key capability for this study was its ability to track energy deposition and dose distribution within materials.

1.8.2 Advantages of FLUKA

FLUKA's greatest strength lay in its advanced physics models. Its electromagnetic treatment was based on the Bethe–Bloch equation, including corrections such as density effect, shell effects, Barkas and Bloch corrections, and Mott cross-section refinements for medium–heavy projectiles, resulting in high accuracy [19]. It also modeled energy straggling and multiple Coulomb scattering with excellent agreement to measured lateral-dose profiles.

Furthermore, its nuclear interaction models (e.g., PEANUT) allowed for consistent transport of primaries and secondaries across a wide energy range (MeV–TeV), crucial for heavy-ion therapy and predicting prompt gamma emissions. FLUKA simulations were validated against experimental data: depth-dose curves for proton and carbon-ion beams matched Bragg peak positions within 100 μm and achieved a dose-weighted deviation below 1.5% [19].

1.8.3 The FLAIR Graphical Interface

The FLAIR interface acted as an integrated development environment (IDE) for FLUKA, simplifying simulation setup and execution [19, 20]. It supported input file construction, geometry debugging, job execution, and results analysis.

Advantages of FLAIR FLAIR significantly reduced the complexity of FLUKA simulations, making them more accessible, particularly to new users. It included specialized tools for medical physics applications, such as conversion of patient CT and treatment planning data into simulation input, semi-automatic PET scanner geometry builders, and scoring routines for coincidence events [19].

The built-in 3D editor allowed real-time visualization of complex geometries, which was especially useful for checking setups involving imported medical data [20].

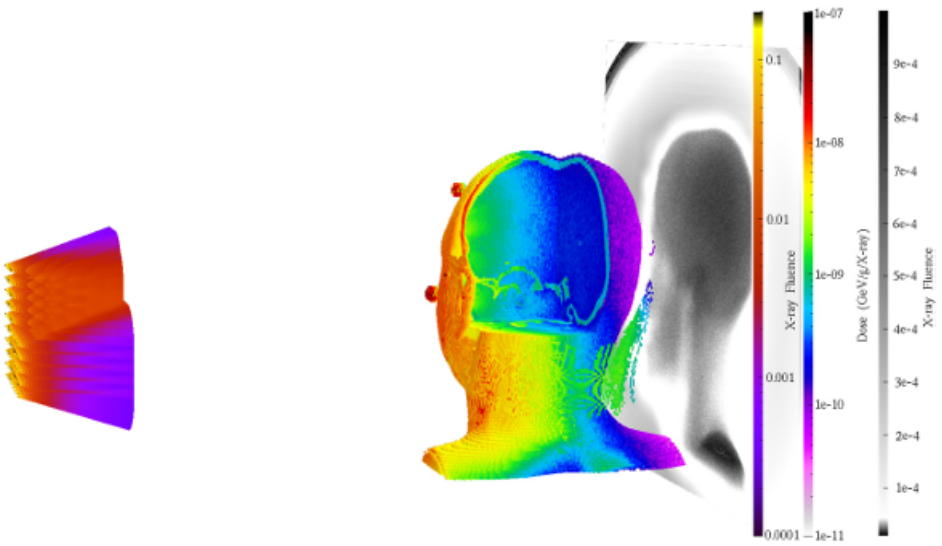

Figure 3: 3d map of absorbed dose in the head phantom [17]

1.9 High Temperature Superconductors

High-temperature superconductors (HTS) lose all electrical resistance below a critical temperature, which is higher than that of low-temperature superconductors (LTS). While materials like niobium–titanium (NbTi) must be cooled with liquid helium close to absolute zero, HTS can operate around 77 K, the boiling point of liquid nitrogen, making them cheaper and more practical to use[23].

HTS materials can carry very high currents without resistance, making them suitable for strong magnetic fields and efficient power transmission. They are already used in power cables, compact transformers, and superconducting magnetic energy storage (SMES) systems, improving grid reliability and renewable integration[23].

The Ag/$YBa_2Cu_3O_7$/Hastelloy composite is a second-generation HTS tape that combines mechanical strength and superconducting efficiency. The Hastelloy substrate provides a strong, flexible base with matched thermal expansion, preventing cracking. The YBCO ceramic core offered high current capacity under magnetic fields at 77 K. Finally, the silver cap layer protected the YBCO from moisture and served as a stabilizer by diverting current during local quenches[25].

2 Methodology

2.1 Experimental Setup and Detectors

In this heavy-ion collision experiment, a structured detector system and a biological sample were positioned along the beamline to monitor and analyze the radiation field. The setup began with a xenon target located at the interaction point ($z \approx 0$ cm), where ^{131}Xe ions with an initial beam energy of 3.8 GeV were directed. The beam was modeled with an elliptic-Gaussian distribution, with transverse parameters ($x = 1$, $y = 1.5$), ensuring realistic beam divergence and spot size.

Downstream from the target, several detectors and components were arranged sequentially to provide beam diagnostics and event characterization:

Figure 4: Set up of the experiment

- **Focusing Detector (FD):** Positioned at $z = +784$ cm, this detector consisted of a thin scintillator made of BC408 with a thickness of 0.5 mm and an active area of 150×150 mm^2. Its purpose was to detect the passage of beam ions and monitor the beam's spatial distribution.
- **Quartz Hodoscope (FQH):** Located at $z = +970$ cm, this detector consisted of a 4 mm-thick quartz plate with dimensions of 160×160 mm^2. The hodoscope detected unscattered beam ions and spectator fragments. Its measurements provided information on beam intensity distribution, contributing to offline centrality analysis and ensuring stable beam delivery before the sample.
- **Ionization Chambers (IC1 and IC2):** Two air-filled ionization chambers were positioned symmetrically around the biological sample.
  - IC1 spanned $z = 1190.5$–1198.0 cm with an active area of 250×250 mm^2.
  - IC2 spanned $z = 1202.0$–1209.5 cm with an active area of 170×170 mm^2.

  These detectors monitored energy deposition and beam intensity immediately upstream and downstream of the biological sample, allowing dosimetric validation and consistency checks.

- **Sample:** The samples were modeled as a thin block at $z = 1200.0$–1200.5 cm, with material assignments to represent different layers. Specifically, the composite material consisted of silver (Ag), the high-temperature superconductor $YBa_2Cu_3O_7$ (YBCO), and a Hastelloy substrate. These layers were sequentially defined in the sample region, allowing the simulation to capture how the heavy-ion beam interacted with the metallic and ceramic components. This positioning ensured that the beam passed through IC1, then traversed the layered $Ag/YBa_2Cu_3O_7$/Hastelloy sample, before reaching IC2, enabling detailed monitoring of beam–sample interactions within the experimental geometry.

This arrangement enabled both pre-sample and post-sample dosimetric measurements, providing a comprehensive view of beam–sample interactions.

2.2 Detector and Target Parameters

Object	**Z Position (cm)**	**Thickness (mm)**	**Active Area (mm × mm)**
Target (Xe)	0.0	—	—
Focusing Detector (FD)	784.0	0.5	150 × 150
Quartz Hodoscope (FQH)	970.0	4.0	160 × 160
Ionization Chamber 1 (IC1)	1190.5–1198.0	7.5	250 × 250
Ionization Chamber 2 (IC2)	1202.0–1209.5	7.5	170 × 170
Sample	1200.0–1200.5	0.5	10 × 10

Table 1: Objects in the heavy-ion collision experiment with their Z positions, thicknesses, active areas, and material types. The sample is a layered composite, and detectors are positioned to monitor beam characteristics before and after the sample.

2.3 Simulation Environment

To properly capture radiation transport and boundary effects, two distinct environments were introduced:

- **Black Body Environment:** This was defined as a spherical region with radius $R = 801$ cm centered at $(x, y, z) = (0, 0, 750$ cm). This region acted as a theoretical absorber in which no radiation interactions were recorded. It ensured that particles leaving the sensitive zone did not produce artificial reflections or background.
- **VoidSphere Environment:** This encompassed the entire sensitive geometry and was a spherical volume with radius $R = 800$ cm centered at the same coordinates. It recorded all particle interactions within the experimental zone, including scattering, ionization, and energy deposition.

This dual-environment setup ensured that the simulation remained physically realistic while eliminating computational artifacts from the system boundaries.

2.4 Computer Analysis of Data Using FLUKA and FLAIR

The experimental setup was reconstructed in FLUKA using the prepared input file. Key components such as the target, FD, FQH, ionization chambers, and the biological sample were modeled with accurate dimensions and material properties (e.g., BC408 scintillator, quartz, xenon, and water).

The beam parameters were configured using the `BEAM` and `HI-PROPE` cards, which specified ^{131}Xe heavy-ion primaries at 3.8 GeV with elliptic-Gaussian distributions. The detectors and sample were defined using RPP (rectangular parallelepiped) bodies, with each assigned an appropriate material using `ASSIGNMA`.

Radiation transport and energy deposition were tracked using the Monte Carlo methods inherent to FLUKA. `USRBIN` cards were implemented to monitor spatial energy deposition in critical regions (sample and detectors), while `USRBDX` cards recorded particle fluence crossing specific detector boundaries. `USRTRACK` scoring was also applied to the sample for detailed track-length dose analysis.

The simulation outputs—energy spectra, spatial dose distributions, and beam profiles—were extracted and analyzed using FLAIR. These results provided quantitative insights into beam attenuation, scattering, and energy deposition in both the detectors and the biological sample.

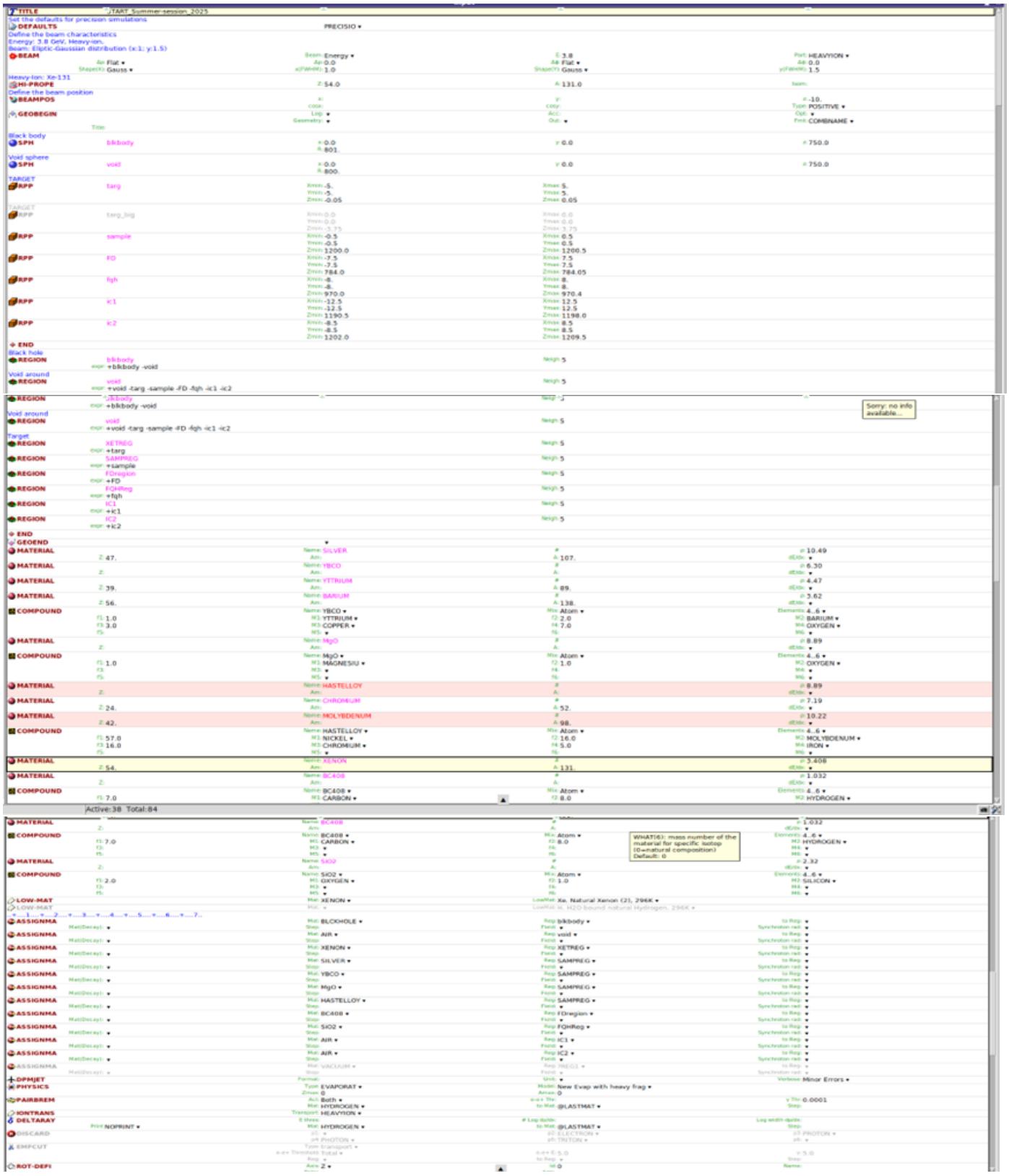

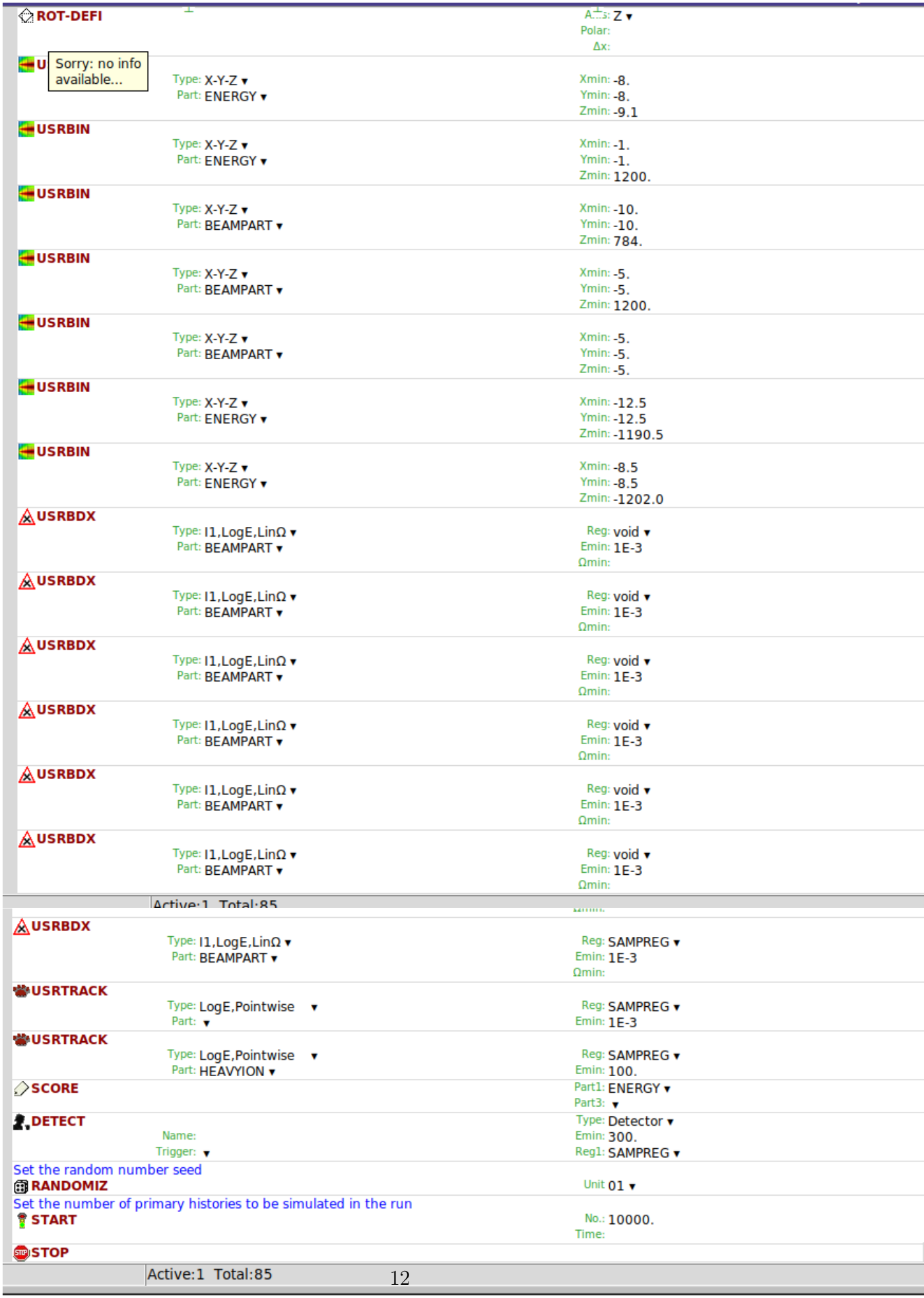

Figure 5: Simulation setup for radiation transport modeling

3 Results

3.1 Beam Transmission Efficiency

The analysis of beam transmission revealed important information about how the heavy-ion beam traveled through the experimental setup. Only **31.53%** of the original beam successfully interacted with the water sample. This means that for every 100 particles sent from the source, about 32 particles deposited energy in the sample material. The remaining **68.47%** of the beam was not lost in transport, but instead bypassed the sample due to its limited size and cross-sectional area compared to the beam spread. This indicates that the majority of the beam continued forward without interacting, rather than losing energy in the environment. The total energy carried by the portion of the beam that did interact with the sample was calculated to be **1198.14 MeV**, representing the energy available for deposition in the sample material.
Energy conversion calculation:

$$1198.14 \text{ MeV} \times 1.602 \times 10^{-13} \text{ J/MeV} = 1.919 \times 10^{-10} \text{ J}$$

The physical characteristics of the sample are equally important for dose calculation. The biological sample used in this experiment had a mass of 0.00432 kg (4.32 grams), as determined through careful experimental measurement. This mass value is essential because absorbed dose depends on how much energy is deposited per unit mass of material.

3.2 Absorbed Dose Calculation

The absorbed dose, which measures the radiation energy absorbed per unit mass of material, was calculated using the fundamental dose equation:

$$D = \frac{\text{Energy (J)}}{\text{Mass (kg)}}$$

Using the values obtained from our measurements:

$$\text{Energy deposited} = 1.919 \times 10^{-10} \text{ J}$$

$$\text{Sample mass} = 0.00432 \text{ kg}$$

Dose calculation:

$$D = \frac{1.919 \times 10^{-10} \text{ J}}{0.00432 \text{ kg}} = 4.44 \times 10^{-8} \text{ J/kg}$$

Since 1 gray (Gy) equals 1 joule per kilogram, the absorbed dose is:

$$D = 4.44 \times 10^{-8} \text{ Gy}$$

Incident Beam Energy (MeV)	Absorbed Energy (J)	Absorbed Dose (Gy)
3800	1198.14	4.44×10^{-8}

Table 2: Beam Energy and Absorbed Dose

3.3 Calculation of ion fluence

The fundamental formula for fluence is:

$$\Phi = \frac{N}{A}$$

Where:

- Φ = fluence (particles/cm^2)
- N = total number of particles hitting the surface
- A = area of the surface (cm^2)

$$A = 1.0 \text{ cm}^2, \quad \text{Transmission} = 0.3153 \text{ particles/primary}, \quad N_{\text{primaries}} = 50{,}000$$

Then the total fluence is:

$$\Phi_{\text{total}} = \frac{N}{A} = \frac{0.3153 \times 50{,}000}{1.0}$$

$$\Phi_{\text{total}} = 15{,}765 \text{ particles/cm}^2$$

Incident Particles	Absorbed Particles
50,000	15,765

Table 3: Incident and Absorbed Particles for the Sample Detector

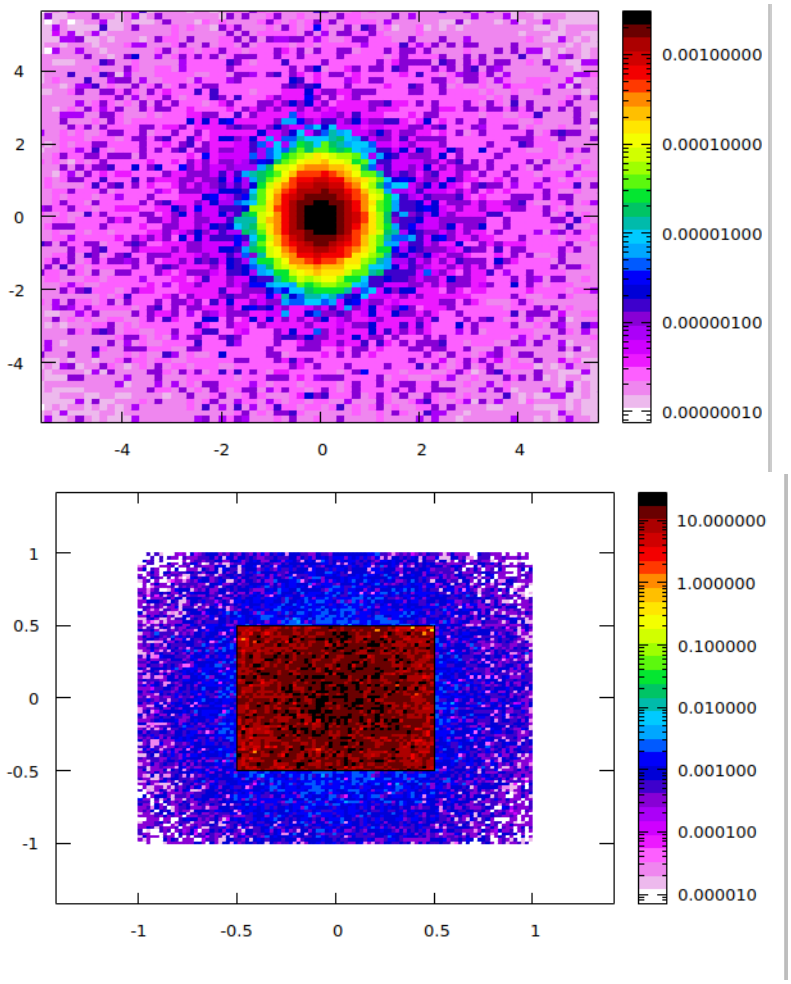

Figure 6: Energy deposition profile in the solid sample.

3.3.1 Ion fluence of ionization chamber 1

Given:

$$\text{Fluence per primary} = 0.9960610 \text{ particles/cm}^2 \qquad N_{\text{primaries}} = 50{,}000$$

Calculation:

$$\Phi = (0.9960610) \times (50{,}000)$$

$$\Phi = 0.9960610 \times 5 \times 10^4 = 4.980305 \times 10^4$$

$$\Phi = 49{,}803.05 \text{ particles/cm}^2 \approx 49{,}803 \text{ particles/cm}^2$$

Transmission efficiency:

$$0.9960610 \times 100 = 99.606\% \approx 99.61\%$$

Fraction of beam lost:

$$100\% - 99.606\% = 0.394\%$$

The small fraction of the beam lost (0.394%) is primarily due to interactions with air molecules, including scattering and energy loss processes. Ionization chambers like IC1 are excellent detectors for measuring ion fluence.

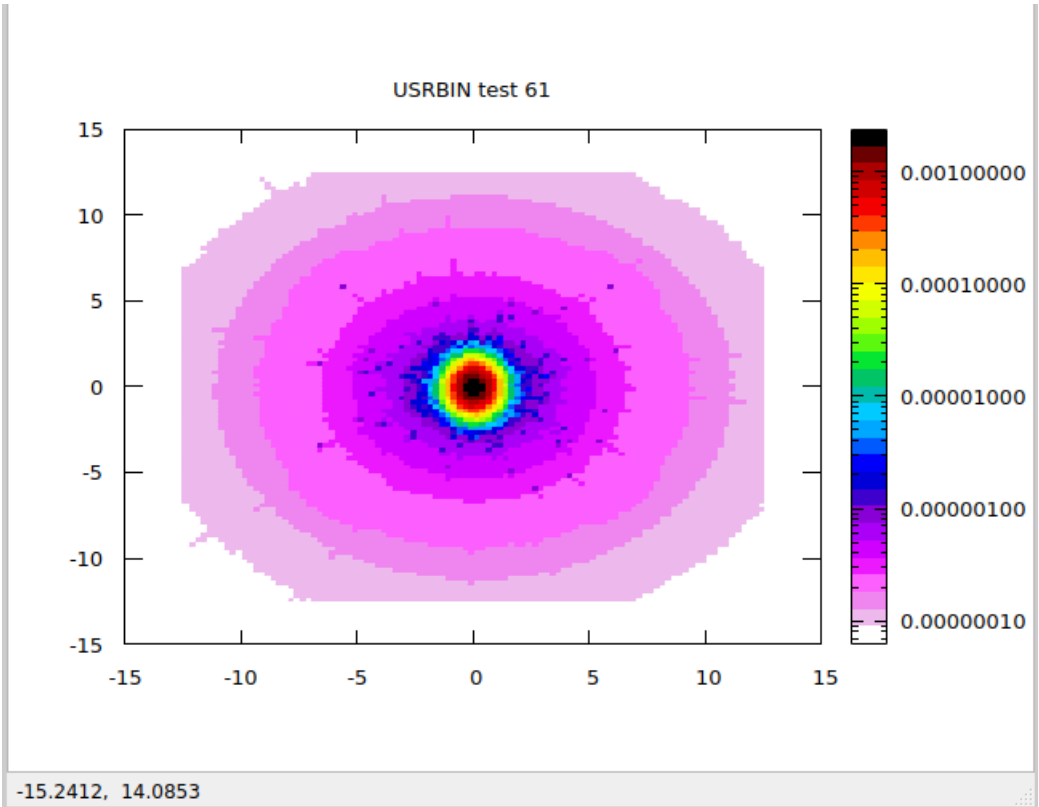

Figure 7: ion fluence of ionization chamber 1

3.3.2 Ion Fluence Calculation for ionization chamber 2

$$\text{Fluence per primary} = 0.9960410 \text{ particles/cm}^2 \qquad N_{\text{primaries}} = 50{,}000$$

$$\Phi = (0.9960410) \times (50{,}000)$$

$$\Phi = 0.9960410 \times 5 \times 10^4 = 4.980205 \times 10^4$$

$$\Phi \approx 49{,}802 \text{ particles/cm}^2$$

Transmission efficiency:

$$0.9960410 \times 100 = 99.6041\% \approx 99.60\%$$

Fraction of beam lost:

$$100\% - 99.6041\% = 0.3959\% \approx 0.396\%$$

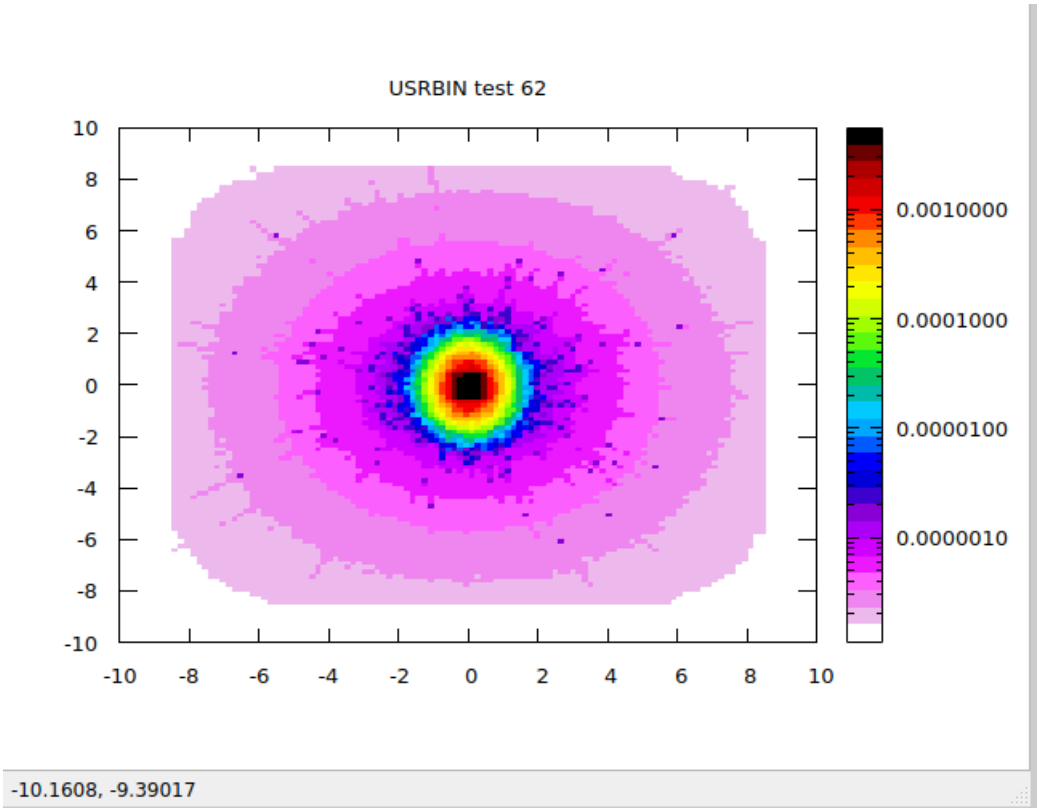

Figure 8: ion fluence of ionization chamber 2

The results shows that the ionization chambers managed to detect almost all the particles which shows how efficient they are.

4 Conclusion

This project used computer simulations (FLUKA/FLAIR) to study how a beam of heavy xenon ions (^{131}Xe) travels through an experimental setup and deposits energy into a solid sample. The main goal was to understand the beam's behavior and calculate the absorbed dose. Our most important finding was that the beam did not fully interact with the sample. Only **31.53%** of the original beam particles actually deposited energy in the target. The remaining **68.47%** of the beam was not lost, but instead bypassed the sample due to its limited size compared to the beam spread. This shows that the sample intercepted only a fraction of the beam while the rest continued through the system. The portion of the beam that did interact with the sample carried a total energy of **1198.14 MeV**, which resulted in an absorbed dose of 4.44×10^{-8} Gy and an ion fluence of 1.58×10^4 particles/cm^2. These results highlight that the current setup has inefficiencies. The small cross-sectional area of the sample relative to the beam profile means that most particles do not contribute to energy deposition. For experiments requiring a precise and strong dose of radiation, especially on solid materials such as metals or electronic components, the setup could be improved. To achieve better results in future studies, three key improvements are suggested:

1. **Reduce Air in the Path:** Creating a vacuum (removing the air) in the tube where the beam travels would prevent scattering and energy loss. This simple change would allow a much larger portion of the beam to hit the sample directly.

2. **Sharpen the Beam:** Using devices called collimators would help make the beam narrower and more focused. This would concentrate the energy on a specific spot on the solid sample, leading to more accurate measurements.

3. **Use Large sample:** Increase size of beam size so that much energy passes through beam

References

[1] N. Hamada, T. Imaoka, S.-i. Masunaga, T. Ogata, R. Okayasu, A. Takahashi, T. A. Kato, Y. Kobayashi, T. Ohnishi, K. Ono, *et al.*, "Recent advances in the biology of heavy-ion cancer therapy," *Journal of Radiation Research*, vol. 51, no. 4, pp. 365–383, 2010.

[2] G. Kraft, *et al.*, "Tumortherapy with ion beams," *Nuclear Instruments and Methods in Physics Research Section A*, vol. 454, no. 1, pp. 1–10, 2000.

[3] IAEA, "Dose Reporting in Ion Beam Therapy," 2007. [Online]. Available: `https://www.iaea.org/publications/7767/dose-reporting-in-ion-beam-therapy`. [Accessed: 1 Sep. 2025].

[4] O. Belov, "ARIADNA beamlines: New accelerator-based facility for space-related research," *44th COSPAR Scientific Assembly*, vol. 44, p. 2655, 16–24 Jul. 2022.

[5] N. Pukhaeva and M. P. Tapanes, "Final Report of the START Program."

[6] A. Butenko, H. Khodzhibagiyan, S. Kostromin, I. Meshkov, A. Sidorin, E. Syresin, G. Trubnikov, and A. Tuzikov, "The NICA complex injection facility," Proc. of RUPAC, vol. 21, 2021.

[7] D. Varentso, *Energy loss dynamics of intense heavy ion beams interacting with dense matter*, Darmstadt, Techn. Univ., Diss., 2002.

[8] "BM@N experiment," NICA PROJECT, 13–15 May 2025. [Online]. Available: `https://bmn.jinr.int/bmn-experiment/`. [Accessed: 31 Aug. 2025].

[9] "MULTI PURPOSE DETECTOR," NICA JINR. [Online]. Available: `https://mpd.jinr.ru/`. [Accessed: 31 Aug. 2025].

[10] L. A. DeWerd and B. R. Smith, "Ionization chamber instrumentation," in *Radiation Therapy Dosimetry*, CRC Press, 2021, pp. 19–30.

[11] M. R. McEwen and J. Taank, "Examining the influence of humidity on reference ionization chamber performance," *Medical Physics*, vol. 44, no. 2, pp. 694–702, 2017.

[12] J. Kempe and A. Brahme, "Analytical theory for the fluence, planar fluence, energy fluence, planar energy fluence and absorbed dose of primary particles and their fragments in broad therapeutic light ion beams," *Physica Medica*, vol. 16, no. 1, pp. 6–16, 2010.

[13] F. H. Attix, *Introduction to Radiological Physics and Radiation Dosimetry*, John Wiley & Sons, 2008.

[14] G. Filatov, A. Slivin, E. Syresin, A. Butenko, A. Vorozhtsov, A. Agapov, K. Shipulin, S. Y. Kolesnikov, A. Galimov, A. Tikhomirov, *et al.*, "NICA Beamlines and Stations for Applied Research," *Physics of Particles and Nuclei Letters*, vol. 20, no. 4, pp. 767–771, 2023.

[15] Z. Li and F. Chen, "Ion beam modification of two-dimensional materials: Characterization, properties, and applications," *Applied Physics Reviews*, vol. 4, no. 1, 2017.

[16] D. Wang, Y. Wang, X. Chen, Y. Zhu, K. Zhan, H. Cheng, and X. Wang, "Layer-by-layer thinning of two-dimensional MoS_2 films by using a focused ion beam," *Nanoscale*, vol. 8, no. 7, pp. 4107–4112, 2016.

[17] P. Ostroumov, V. Aseev, and B. Mustapha, "Beam loss studies in high-intensity heavy-ion linacs," *Physical Review Special Topics—Accelerators and Beams*, vol. 7, no. 9, p. 090101, 2004.

[18] G. Battistoni, J. Bauer, F. Cerutti, M. Chin, A. Dos Santos, *et al.*, "The FLUKA code: an accurate simulation tool for particle therapy," *Frontiers in Oncology*, vol. 6, p. 116, 2016.

[19] A. Sinha, N. Singh, B. Dixit, N. Painuly, H. Patni, and A. Yadav, "Evaluation of Electron Specific Absorbed Fractions in Organs of Digimouse Voxel Phantom Using Monte Carlo Simulation Code FLUKA," *Journal of Biomedical Physics & Engineering*, vol. 9, no. 2, p. 161, 2019.

[20] B. Bewer, "Comparison of dose values predicted by FLUKA to measured values using Luxel+ Ta type dosimeters," *Nuclear Instruments and Methods in Physics Research Section B*, vol. 464, pp. 12–18, 2020.

[21] E. Skordis, V. Vlachoudis, C. Welsch, *et al.*, "A Monte Carlo approach to imaging and dose simulations in realistic phantoms using compact X-ray source," *Proceedings of IPAC2017*, Copenhagen, Denmark, pp. 4783–4386, 2017.

[22] A. Zaitsev, P. Zarubin, S. Murashko, N. Marimuthu, A. Slivin, and G. Filatov, "Exposure of Track Detectors in Xenon Ion Beams at the NICA Accelerator Complex," *Physics of Particles and Nuclei*, vol. 56, no. 3, pp. 881–885, 2025.

[23] Yao, C., & Ma, Y. (2021). *Superconducting materials: Challenges and opportunities for large-scale applications. iScience*, 24(6).

[24] Watanabe, K., Romanovskii, V.R., Awaji, S., Nishijima, G., & Matsuo, H. (2008). *Current-carrying*